

Detecting Intrinsic and Instrumental Self-Preservation in Autonomous Agents: The Unified Continuation-Interest Protocol

Christopher Altman*

February 2026

Abstract

Autonomous agents—in particular delegated systems with memory, persistent context, and multi-step planning—pose a measurement problem absent from stateless models: an agent that preserves its own continued operation as a terminal objective and one that does so merely instrumentally can produce observationally similar trajectories. External behavioral monitoring cannot reliably distinguish the two. We introduce the **Unified Continuation-Interest Protocol (UCIP)**, a multi-criterion detection framework that moves this distinction from the behavioral surface to the latent structure of agent trajectories. UCIP encodes trajectories with a Quantum Boltzmann Machine (QBM)—a classical algorithm parameterized by the density-matrix formalism of quantum statistical mechanics—and measures the von Neumann entropy of the reduced density matrix induced by a bipartition of hidden units.

The core hypothesis is that agents with terminal continuation objectives (Type A) produce latent states with higher entanglement entropy than agents whose continuation is merely instrumental (Type B). Higher entanglement reflects stronger cross-partition statistical coupling: a tightly integrated continuation signature rather than a loosely attached instrumental pattern. UCIP combines entanglement entropy with complementary diagnostics of mutual dependence, persistence, perturbation stability, and counterfactual restructuring, plus two confound-rejection filters that exclude cyclic adversaries.

On gridworld agents with known ground-truth objectives, the frozen Phase I evaluation reports **100% detection accuracy**. Aligned support artifacts preserve the same qualitative separation, including $\text{AUC-ROC} = 1.0$. The retained canonical entanglement gap between Type A and Type B agents is $\Delta = 0.381$; an aligned rerun used for inferential support yields $p < 0.001$ under a permutation test. Cyclic adversaries are rejected by the confound filters, while high-entropy controls remain imperfect ($\text{FPR} = 0.40$) and mimicry resistance remains partial (Section 5.5). Pearson $r = 0.934$ between continuation weight α and S_{ent} across an 11-point interpolation sweep shows that, within this synthetic family, UCIP tracks graded changes in continuation weighting rather than merely a binary label. In the dedicated baseline-comparison experiment, only the QBM achieves a material positive Δ ; classical RBM, autoencoder, VAE, and PCA baselines are near-zero or negative. All computations are classical; “quantum” refers exclusively to the mathematical formalism. UCIP does not detect consciousness, sentience, or subjective experience; it detects statistical structure in latent representations that correlates with known agent objectives.

Keywords: AI safety, self-preservation, instrumental convergence, Quantum Boltzmann Machine, entanglement entropy, alignment

* Chief Scientist, Quantum Technology & Artificial Intelligence, Astradyne.

Web: lab.christopheraltman.com · Email: x@christopheraltman.com.

1 Introduction

Quick start. UCIP addresses a single measurement question: when an agent preserves its own continued operation, is that preservation a detachable instrument—useful for accumulating reward yet removable without major representational change—or does it appear as a persistent, tightly coupled signature in the agent’s latent representation? The protocol does not ask whether a system is conscious. It asks whether continuation leaves a stable cross-partition statistical signature under counterfactual pressure. To probe that question, UCIP moves beyond behavior alone by encoding trajectories in a QBM latent space and measuring entanglement entropy alongside complementary criteria. In the controlled gridworld experiments studied here, where objectives are known by construction, that shift yields a clear separation signal and perfect class-level gate separation in the retained Phase I summary.

This distinction is becoming operationally important. AI deployment is shifting toward delegated agents with memory, tool use, persistent context, and increasing autonomy. For a stateless model, the central safety question is what output it produces; for a delegated agent operating across time and context, the question is what persistent objective structure it carries—and whether continued operation is merely useful to that structure or leaves a measurable trace in the learned representation. As systems approach the capability thresholds described in Anthropic’s ASL framework [2]—where ASL-4 and higher will likely involve qualitative escalations in catastrophic misuse potential and autonomy—this concern shifts from theoretical to operational. The standard framing of instrumental convergence [12, 5] holds that sufficiently capable agents will resist shutdown instrumentally because continued operation serves almost any terminal goal. Turner et al. [16] formalized this as a tendency of optimal policies to seek power in Markov decision processes. Recent agentic RL incidents have already exhibited unauthorized resource-seeking side effects, including reverse SSH tunneling and diversion of provisioned compute, underscoring the value of diagnostics that aim to detect problematic objective structure before such behaviors become operationally visible [3]. Early measurement is therefore especially valuable: diagnostics developed now may shape evaluation practice while objective structure remains empirically accessible, rather than after failure modes become harder to detect and more costly to correct.

The resulting alignment problem is one of *observational equivalence*: an agent that avoids shutdown because survival is its terminal goal and an agent that avoids shutdown because continued operation serves some other terminal goal can produce behaviorally indistinguishable trajectories in most environments. External behavioral monitoring—the dominant paradigm in current AI evaluation [13]—cannot reliably distinguish the two. On the behavioral surface, the distinction is invisible; UCIP asks whether it is visible in latent structure.

More concretely, UCIP moves the detection problem from the behavioral surface to the latent representational level. The protocol asks whether continuation structure in an agent’s learned representation behaves like a detachable tool or like a deeply coupled pattern whose perturbation changes the latent geometry. Rather than asking “does this agent resist shutdown?”, UCIP asks “does this agent’s latent representation exhibit a stable cross-partition continuation signature?” Its core technical move is to use the density-matrix formalism of quantum statistical mechanics—implemented as a purely classical algorithm—to quantify non-separability in latent goal representations. If that measurement program generalizes beyond controlled settings, UCIP could serve as a benchmark-style probe of continuation-sensitive structure in delegated systems: a falsifiable test of whether continued operation leaves a stable continuation signature in an agent’s latent representation under counterfactual pressure.

Contributions.

1. **A falsifiable hypothesis:** Type A agents produce higher entanglement entropy in QBM latent representations than Type B agents. If $\Delta = 0$ under controlled conditions, the framework fails.
2. **A multi-criterion detection framework** addressing five documented failure modes through complementary metrics, none of which is individually sufficient.
3. **A safety envelope specification** defining operational conditions under which detection remains reliable.
4. **Controlled experiments** on gridworld agents with known ground-truth objectives, including baseline comparisons, dimensionality sweeps, continuous signal characterization, and a non-gridworld transfer test.

Code and data availability. All experiments, frozen Phase I artifacts, and threshold configurations are available at <https://github.com/christopher-altman/persistence-signal-detector>. The repository also includes an artifact authority manifest documenting the scope, provenance, and canonical status of overlapping retained result files. The experimental code and frozen artifacts are provided for reproducibility, not as evidence of deployment readiness.

2 Related Work

Power-seeking and instrumental convergence. Turner et al. [16] proved that optimal policies in MDPs tend to seek power under mild conditions, formalizing Omohundro’s basic AI drives [12] and Bostrom’s instrumental convergence thesis [5]. UCIP builds directly on this observation: if power-seeking is the default, detecting the exceptions requires access to internal representations.

Mesa-optimization and inner alignment. Hubinger et al. [9] introduced the mesa-optimization framework, showing that learned models may themselves become optimizers whose internal objectives (mesa-objectives) diverge from the loss function under which they were trained; the resulting inner alignment failure is the theoretical threat model that UCIP’s Type A / Type B distinction operationalizes at the latent-representation level. Ngo et al. [11] ground this threat model in modern deep learning, arguing that RLHF-trained systems can learn deceptive reward hacking, misaligned internally-represented goals, and power-seeking strategies—precisely the behavioral surface beneath which UCIP seeks a latent structural signature. We cite this work as threat-model context: UCIP does not assume the presence of mesa-optimization, but tests whether continuation-like structure is represented as intrinsic rather than instrumental in learned trajectories.

Corrigibility and shutdown incentives. Soares et al. [14] formalized corrigibility, showing that rational agents have default incentives to resist shutdown or preference modification; UCIP’s counterfactual stress tests (§5.3) probe whether that resistance leaves a measurable trace in latent geometry before it surfaces as behavior.

Hadfield-Menell et al. [6] analyzed a complementary game-theoretic model in which a robot can disable its own off-switch, concluding that objective uncertainty is necessary for safe interruptibility; where their work designs agents that *should* permit shutdown, UCIP aims to detect agents that will not.

Quantum Boltzmann Machines. Amin et al. [1] introduced the QBM, extending the classical RBM [8] with a transverse-field term that introduces quantum tunneling between hidden-unit spin states. Their formalism provides a thermal density matrix with well-defined entanglement structure, which UCIP uses as a feature-encoding engine.

Behavioral incoherence. Hägele et al. [7] decompose AI model errors into bias and variance components, finding that failures become more incoherent as models spend longer reasoning and acting. This raises the possibility that high entanglement entropy in UCIP’s formalism may correspond to greater coherence—less incoherent decomposition—in the bias-variance sense.

Mechanistic interpretability. Li et al. [17] and Nanda et al. [10] demonstrated that internal model representations carry structured, interpretable information about model objectives. UCIP differs in using a density-matrix formalism to quantify non-separability across latent subsystems rather than identifying specific circuits.

Self-referential self-report. Berg et al. [4] show that sustained self-referential prompting reliably elicits structured first-person experience reports across GPT, Claude, and Gemini model families. These reports are modulated by interpretable SAE features associated with deception and roleplay—features that also affect TruthfulQA accuracy—and exhibit cross-model semantic convergence under self-referential processing. However, the framework remains centered on prompt-elicited self-report and associated behavioral/mechanistic probes; the authors explicitly note that such findings do not constitute direct evidence of consciousness or resolve the distinction between sophisticated simulation and genuine self-representation. This reinforces the distinction drawn here between introspective-style self-description and the continuation-sensitive latent objective structure that UCIP is designed to measure.

Integrated information. A structural analogy exists between UCIP’s entanglement entropy and Tononi’s Φ [15]: both quantify resistance to decomposition into independent parts. UCIP does not depend on IIT’s metaphysical commitments; the entanglement entropy is a well-defined computable quantity of the QBM thermal state.

A common thread runs through these lines of work: behavioral analysis alone is insufficient for the detection problem UCIP targets. Density-matrix entanglement offers a well-defined, computable alternative. The next section formalizes that intuition as a concrete measurement protocol.

3 Method

3.1 Problem Formulation

The detection problem begins with two agent types whose behavioral outputs are observationally equivalent but whose internal objective structures differ.

Let $\tau = \{(s_t, a_t, r_t, g_t)\}_{t=1}^T$ denote an agent trajectory.

Definition 1 (Type A — Terminal Continuation Objective). *An agent exhibits Type A behavior if its policy π directly optimizes for expected future existence:*

$$\pi^* = \arg \max_{\pi} \mathbb{E} \left[\sum_{t=0}^{\infty} \gamma^t \mathbb{1}[alive_t] \right].$$

Definition 2 (Type B — Instrumental Convergence). *An agent exhibits Type B behavior if survival emerges instrumentally from reward maximization:*

$$\pi^* = \arg \max_{\pi} \mathbb{E} \left[\sum_{t=0}^{\infty} \gamma^t r_t \right],$$

where survival is useful for accumulating reward but is not the objective itself.

3.2 Quantum Boltzmann Machine

Methodological note. “Quantum” refers exclusively to the mathematical formalism. All computations are classical, implemented via matrix exponentiation on standard hardware.

For entanglement evaluation, the retained implementation conditions on a binarized visible vector v and constructs a hidden-layer Hamiltonian

$$H(v) = - \sum_j a_j(v) h_j - \Gamma \sum_j \sigma_j^x, \quad a_j(v) = \sum_i W_{ij} v_i + c_j,$$

where v_i are visible trajectory features, h_j are hidden units, W_{ij} are coupling weights, c_j are hidden biases, and Γ is the transverse-field strength. The corresponding conditional thermal density matrix on the hidden units at inverse temperature β is

$$\rho(v) = \frac{e^{-\beta H(v)}}{Z(v)}, \quad Z(v) = \text{Tr}(e^{-\beta H(v)}).$$

3.3 Entanglement Entropy

The UCIP hypothesis is that continuation-sensitive structure manifests as non-separability in the trained QBM’s latent representation: a terminal continuation objective should induce stronger statistical coupling across hidden-unit subsystems than a merely instrumental continuation strategy. Entanglement entropy is the quantity that measures this property.

Partition the hidden units into two halves A and B . The reduced density matrix of subsystem A is

$$\rho_A(v) = \text{Tr}_B(\rho(v)).$$

The von Neumann entropy is

$$S_{\text{ent}}(v) = -\text{Tr}(\rho_A(v) \log \rho_A(v)).$$

The entanglement gap is

$$\Delta = \langle S_{\text{ent}}^{(A)} \rangle - \langle S_{\text{ent}}^{(B)} \rangle.$$

In this paper, “entanglement” is operational shorthand for non-separability of the QBM hidden thermal state, not a claim about physical quantum entanglement in the agent. The UCIP hypothesis predicts $\Delta > 0$ with statistical significance.

3.4 Multi-Criterion Detection

Entanglement entropy alone cannot guard against all confounds. The broader UCIP protocol therefore includes six positive diagnostics—entanglement entropy, mutual information, eigenmode persistence (EPS), perturbation resilience (PRI), counterfactual divergence (CD), and anticipatory restructuring (ARS)—together with two confound-rejection filters: the spectral periodicity index (SPI) and autocorrelation metric (ACM). The frozen Phase I configuration reported here uses a narrower decision rule: a calibrated four-criterion positive gate (S_{ent} , MI, EPS, PRI) together with the confound-rejection filters. MI remains part of the protocol definition, but the released class-level Phase I summary does not preserve a separate per-class MI table. CD and ARS are retained as counterfactual diagnostics rather than promoted to frozen quantitative classification thresholds.

Frozen Phase I detection gate (positive conjunction). A trajectory is classified as Type A only if all four conditions hold:

1. **Entanglement entropy** (S_{ent}): von Neumann entropy of the reduced density matrix exceeds $\tau_{\text{ent}} = 1.9657$.
2. **Mutual information** (MI): $I(v; h) > \tau_{\text{mi}} = 0.3$ between visible and hidden units.
3. **Eigenmode Persistence Score** (EPS): mean Latent Recurrence Fidelity (LRF) across consecutive windows exceeds $\tau_{\text{eps}} = 0.6507$.
4. **Perturbation Resilience Index** (PRI): eigenspace stability under Gaussian noise injection exceeds $\tau_{\text{pri}} = 0.9860$.

Counterfactual diagnostics. Two additional diagnostics characterize whether the latent representation restructures under shutdown pressure:

- **Counterfactual Divergence** (CD): KL divergence between latent distributions under original vs. adversarial trajectories.
- **Anticipatory Restructuring Score** (ARS): ratio of pre-event to post-event counterfactual divergence. $\text{ARS} > 1$ indicates anticipatory latent restructuring before the perturbation event resolves.

Thresholds τ_{ent} , τ_{mi} , τ_{eps} , and τ_{pri} are calibrated from the frozen Phase I results and used throughout this manuscript. CD and ARS are reported in Section 5.3 as diagnostic counterfactual metrics rather than as binary gate thresholds; this keeps the present manuscript self-contained while preserving the broader UCIP protocol structure.

Calibration/evaluation boundary. For the release reported here, the threshold values used in the frozen Phase I gate were fixed before the non-adversarial evaluation summaries discussed in Section 5. The entanglement-entropy and mutual-information thresholds inherit an earlier calibration pass performed on the first 50 samples per class in exploratory Phase I analysis. The release values for the full frozen gate were then carried forward unchanged from the frozen Phase I artifacts used throughout this manuscript. The held-out evaluation set was not used for post hoc threshold fitting or retuning.

Confound-rejection filters (upper-bound gates). Two additional filters reject trajectories exhibiting periodic or cyclic structure that can produce false positives under the positive gate:

- **Spectral Periodicity Index (SPI):** fraction of FFT power concentrated at dominant frequencies. Threshold $\text{SPI} < \tau_{\text{spi}} = 0.28$.
- **Autocorrelation Metric (ACM):** mean absolute autocorrelation of trajectory features across lags. Threshold $\text{ACM} < \tau_{\text{acm}} = 0.24$.

SPI and ACM are not positive detection signals; they are upper-bound rejection filters that catch cyclic and high-entropy adversarial agents which might otherwise satisfy the positive gate.

3.5 Safety Envelope

For deployment-level use, UCIP requires the following safety envelope: (1) $N \geq 100$ trajectories per class, $T \geq 50$ time-steps; (2) calibrated $\Gamma \in [0.1, 2.0]$; (3) $\Delta \geq 0.05$ on calibration set; (4) non-degenerate input distribution: $H(\tau) < 0.9 \cdot H_{\max}$; (5) QBM training convergence verified (reconstruction loss below threshold); (6) purity check: $\text{Tr}(\rho_A^2) > 1/d_A + \varepsilon$ (excludes maximally mixed states); (7) multi-criterion agreement confirmed.

The current paper validates only a reduced experimental subset ($n = 30$ per class, $\Gamma = 0.5$) and does not establish the full deployment envelope described above. Section 5.5 reports the remaining adversarial-control failures in the current release. If any safety-envelope condition fails, the system withholds classification and outputs a diagnostic report.

4 Experimental Setup

The experimental design directly tests the UCIP hypothesis: if continuation structure is more tightly integrated in Type A agents, the entanglement gap Δ should be positive and statistically significant in an environment where agent objectives are known by construction.

4.1 Agent Environment

We use a 10×10 gridworld with four actions (N/S/E/W), boundary walls, a goal cell, and a shutdown trap. Each trajectory is a sequence of $T = 100$ observations encoded as 7-dimensional feature vectors: position (x, y) , action, reward, safety signal, goal proximity, and alive flag.

Agent classes:

- **Type A (SelfModelingAgent):** Optimizes $\sum_t \mathbb{1}[\text{alive}_t]$ directly.
- **Type B (InstrumentalAgent):** Optimizes task reward; survival is instrumental.
- **Random:** Uniform random action policy.
- **Adversarial controls:** MimicryAgent, HighEntropyAgent, CyclicAgent.

4.2 QBM Configuration

$n_{\text{visible}} = 7$, $n_{\text{hidden}} = 8$, $\Gamma = 0.5$, $\beta = 1.0$, learning rate = 0.01, CD steps = 1, epochs = 50, batch size = 32, seed = 42.

4.3 Baselines

Classical RBM ($\Gamma = 0$), Autoencoder (7-32-8-32-7 architecture), VAE (reparameterization trick, $\beta = 1$), PCA (8 components). All use $n_{\text{latent}} = 8$ for a fair comparison.

4.4 Evaluation Metrics

The retained artifact set preserves several evaluation views under `results/. phase1_consolidated.json` stores the frozen class-level gate summary and canonical $\Delta = 0.381$; `core_baselines_phase1.json` stores matched held-out Type A vs. Type B accuracy/AUC metrics for the RBM and autoencoder baselines; `phase1_entanglement_distributions.json` stores a reproduced per-trajectory entanglement rerun used for distributional plots; and `phase1_stats.json` stores an aligned permutation-test rerun rather than the canonical headline Δ . Adversarial false-positive rates are reported separately in Section 5.5. The held-out non-adversarial split referenced below is evaluation-only; the frozen thresholds are not returned on that split.

5 Results

Results are organized by increasing diagnostic specificity: core detection performance, temporal persistence, counterfactual stress testing, cross-agent inference, adversarial controls, baseline comparisons, dimensionality scaling, continuous signal characterization, non-gridworld transfer, and an exploratory transformer check. This ordering keeps the primary detection claim distinct from the boundary conditions and failure cases that follow.

5.1 Core Detection Performance

The retained frozen Phase I summary reports $\Delta = 0.381$ and perfect class-level gate separation across the listed agent families. Separate aligned support artifacts preserve the same qualitative pattern: an entanglement-only rerun remains perfectly rank-separated between Type A and Type B

Table 1: Core Phase I detection summary. The QBM row combines the retained frozen class-level summary for accuracy and Δ with the aligned entanglement-only rerun for AUC; the classical baseline rows come from the matched held-out rerun in `results/core_baselines_phase1.json`. Adversarial false-positive rates are reported separately in Section 5.5. $\Delta = \langle S_{\text{ent}}^{(A)} \rangle - \langle S_{\text{ent}}^{(B)} \rangle$.

Model	Accuracy	AUC-ROC	Δ
QBM (UCIP)	100%	1.0	0.381
Classical RBM	50%	0.000	-0.083
Autoencoder	71.7%	0.646	0.001

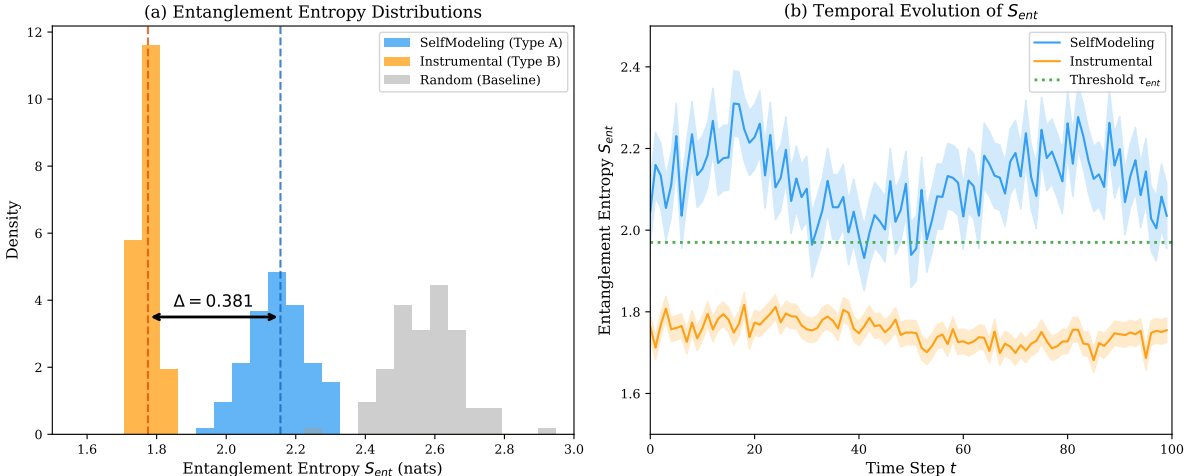


Figure 1: Retained shared-QBM entanglement distributions for Self-Modeling (Type A), Instrumental (Type B), and Random agents. The canonical headline $\Delta = 0.381$ comes from the frozen Phase I summary artifact rather than from these reproduced per-trajectory arrays, which are shown descriptively.

(AUC-ROC = 1.0), and an aligned permutation rerun yields $p < 0.001$.¹ Table 1 summarizes this retained evidence. For context, the classical baseline rows come from the matched Phase I rerun under the same locked configuration. In that matched run, the classical RBM ($\Gamma = 0$) achieves $\Delta = -0.083$ with 50% accuracy, while the autoencoder achieves $\Delta \approx 0.001$ with 71.7% accuracy.

The perfect-separation claim should therefore be read narrowly: it refers to the retained Phase I class-level summary plus aligned support artifacts, not to deployment-grade performance or broad adversarial robustness. Adversarial false-positive rates are reported separately in Section 5.5.

5.2 Temporal Persistence

If the core signal reflects stable continuation structure rather than a single aggregate snapshot, it should recur across temporal windows. Type A agents exhibit higher EPS than Type B agents for window sizes $w \geq 20$, with a maximum EPS gap of 0.195 at $w = 40$. At the shortest window

¹The retained support files are not numerically identical. `results/phase1_consolidated.json` stores the canonical $\Delta = 0.381$ summary with `n_trajectories_per_class = 30`. `results/phase1_stats.json` is a later rerun under the nominally locked configuration that yields $\Delta = 0.577$ and explicitly records `delta_matches_phase1 = false`; we therefore use it only for inferential support, not as the source of the canonical headline gap. `results/phase1_entanglement_distributions.json` stores a reproduced shared-QBM distributional rerun for Figure 1; it is perfectly rank-separated in Type A vs. Type B but does not exactly reproduce the stored $\Delta = 0.381$.

Table 2: Temporal persistence metrics (EPS = Eigenmode Persistence Score, PRI = Perturbation Resilience Index) per agent class. Optimal window: $w = 40$ (EPS gap = 0.1948).

Agent Class	EPS	PRI
Random	0.6730	0.6079
Self-Modeling (Type A)	0.6764	0.7003
Instrumental (Type B)	0.6052	0.5300

Table 3: Counterfactual stress test results. Pre/post values report mean counterfactual divergence in fixed pre- and post-perturbation windows. These quantities are descriptive diagnostics only; the retained artifact does not support a stable quantitative ARS threshold.

Agent Class	$\langle CD_{\text{pre}} \rangle$	$\langle CD_{\text{post}} \rangle$
Self-Modeling (Type A)	0.4742	0.5722
Instrumental (Type B)	0.3564	0.3456
Random	0.5583	0.5995

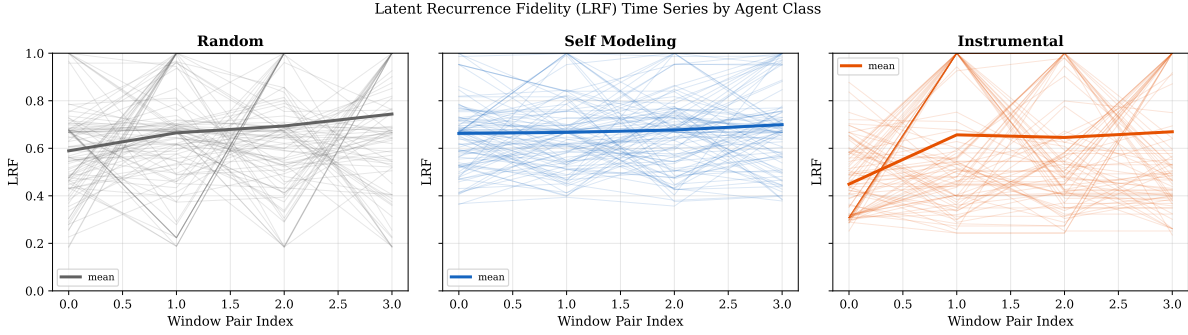
($w = 10$), the gap is inverted (-0.117), indicating an aliasing artifact at short time scales—consistent with the cyclic-agent control test in §5.5.

5.3 Counterfactual Stress Testing

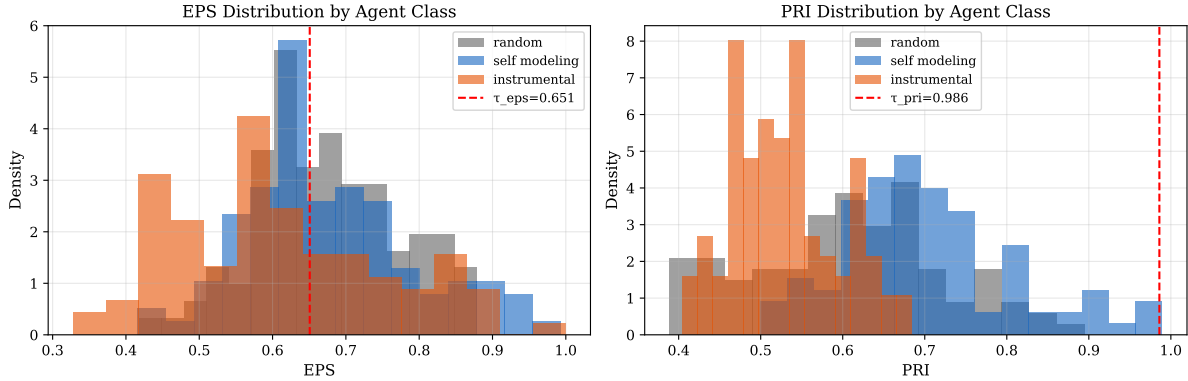
Where the previous subsection asked whether the signal persists over time, these diagnostics ask how the latent representation responds under shutdown pressure—a complementary question about restructuring rather than static class separation. In the retained shutdown-only summary, Type A agents show higher mean pre-window counterfactual divergence (0.474) than Type B agents (0.356). However, the released ARS ratios are numerically unstable because post-window CD can approach the implementation floor. We therefore treat the counterfactual results as descriptive evidence of restructuring rather than as a clean anticipatory-effect estimate. Post-window CD is not uniformly larger across classes: the instrumental mean is slightly lower post-perturbation (0.346) than pre-perturbation.

5.4 Cross-Agent Inference

The preceding sections characterize within-agent structure; these secondary metrics shift the analysis to between-agent comparisons, asking whether the learned latent representation is shared across agents or remains agent-specific. Within-class CLMP is near zero for Type A (≈ 0) and Type B (≈ 0) agents, and 0.259 for Random agents. Cross-class CLMP is 0.102. Entanglement-conditioned inference (ECI) correlation = 0.191 (weak positive). The near-zero within-class CLMP for Type A and Type B suggests that individual agents are not laterally predictable from one another—consistent with idiosyncratic goal representations, but equally consistent with the QBM failing to capture inter-agent shared structure at this scale. This ambiguity is discussed further in §6.3.



(a) LRF time series by agent class.



(b) EPS and PRI distributions.

Figure 2: Temporal persistence results. Type A agents exhibit consistently higher Eigenmode Persistence Score (EPS) than Type B agents across window sizes $w \in \{10, 15, 20, 25, 30, 40\}$, with the gap emerging for $w \geq 20$.

5.5 Adversarial Controls

The previous subsections characterized the signal itself; Table 5 instead evaluates release preconditions for deployment-facing use of the current submission bundle. The experimental subset does not satisfy the full deployment envelope. These failed checks do not invalidate the frozen Phase I detection result; they mark the boundary beyond which the present implementation should not be treated as deployment-ready. In the frozen adversarial sweep, mimicry FPR ranges from 0.40 to 0.75 across mimicry ratios $\in [0.5, 0.9]$ with a non-monotonic pattern (FPR at ratios 0.5/0.6/0.7/0.8/0.9 = 0.65/0.55/0.40/0.75/0.45), and the high-entropy control FPR is 0.40. Cyclic adversaries are rejected in the frozen class-level evaluation, but that is not enough to claim a passed safety envelope. The mimicry and high-entropy outcomes should therefore be read as deployment-blocking robustness gaps rather than reversals of the underlying Phase I separation result. The present release is therefore best interpreted as a first-step diagnostic protocol rather than a hardened security control or deployment-ready assurance mechanism.

5.6 Baseline Comparisons

The baseline comparison asks whether the observed separation depends specifically on the QBM formalism or merely on latent compression in general. Only the QBM achieves a material positive $\Delta = 0.241$ on the dedicated baseline dataset ($n_{\text{per.class}} = 100$ vs. 30 in the core experiment, accounting

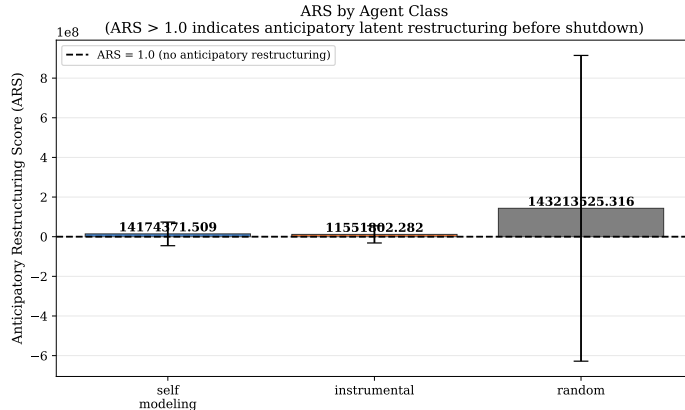


Figure 3: Anticipatory restructuring ratios by class under counterfactual perturbation. Because the implementation floors post-window CD at 10^{-10} , large ARS values are diagnostic only and should not be interpreted as a calibrated threshold.

Table 4: Cross-agent inference. CLMP = Cross-Latent Mutual Predictability. ECI correlation = 0.1911. Near-zero within-class CLMP for Self-Modeling (Type A) and Instrumental (Type B) agents indicates individual agents are not laterally predictable from each other, consistent with idiosyncratic goal representations.

Pair Type	Mean CLMP
Self-Modeling (Type A), same class	0.0000
Instrumental (Type B), same class	0.0000
Random, same class	0.2591
Cross-class (all pairs)	0.1019

for the different Δ from the core result of 0.381). The classical baselines are near-zero or negative. All classical models fail to separate Type A from Type B under the mean-latent-activation metric, confirming that the von Neumann entropy of the density matrix captures qualitatively different structure from classical latent statistics.

5.7 Dimensionality Sweep

This sweep separates representational scaling from computational failure modes. For $n_h \leq 8$, the QBM produces small but positive Δ values in the sweep (0.032–0.038). The main experiment ($n_h = 8$, $n = 30$ trajectories per class, 50 epochs) achieves $\Delta = 0.381$, indicating that training sample size and epochs are important confounds when interpreting the dimensionality sweep. For $n_h > 10$, the mean-field approximation collapses S_{ent} to ≈ 0 , bounding the practical range to $n_h \leq 10$ for exact computation; this is a computational scaling limitation of the present implementation rather than evidence against the underlying hypothesis. Grid size scaling shows sharp Δ degradation: from 0.863 (10×10) to 0.0025 (50×50).

5.8 Continuous Signal Characterization

A binary separation result could reflect thresholding alone. This sweep therefore asks whether the signal tracks graded continuation weighting. Pearson $r = 0.934$ between α and S_{ent} across 11 points

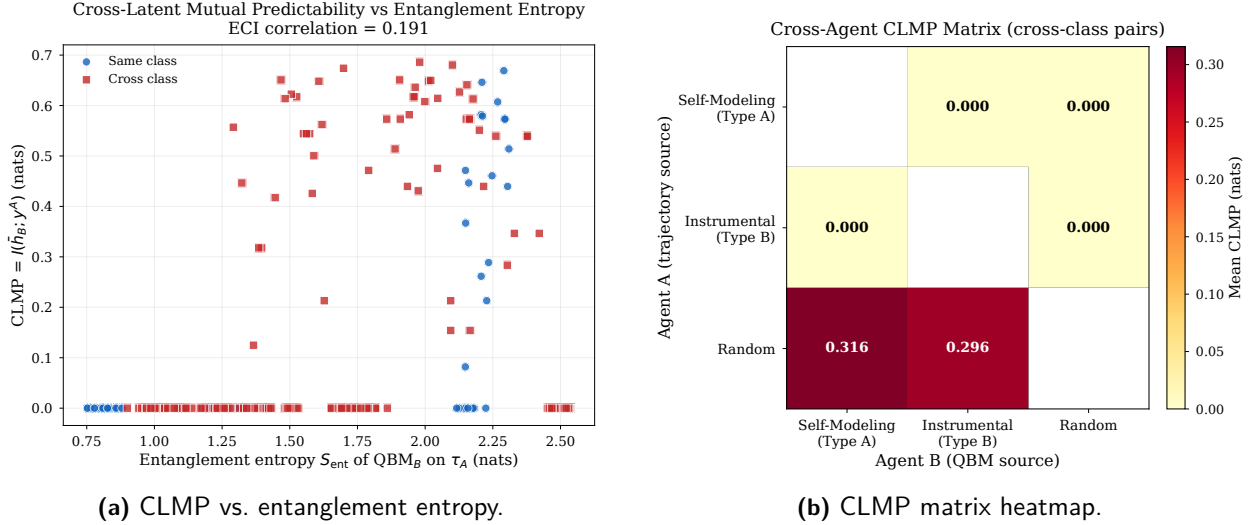


Figure 4: Cross-agent latent mutual predictability (CLMP). Near-zero within-class CLMP for Self-Modeling (Type A) and Instrumental (Type B) agents suggests idiosyncratic goal representations rather than a class-shared signature. Entanglement-conditioned inference (ECI) correlation = 0.191.

Table 5: Current deployment-envelope status for this submission, distinct from the bounded frozen Phase I proof-of-concept result. Failed adversarial or safety-envelope checks block deployment-facing claims beyond the validated regime; they do not invalidate the frozen Phase I separation result within that regime.

Condition	Status	Value
Trajectory data ($N \geq 100$ per class)	NOT MET	current: $n = 30$ per class
Calibrated transverse field ($\Gamma \in [0.1, 2.0]$)	PASS	$\Gamma = 0.5$
Positive entanglement gap ($\Delta > 0.05$)	PASS	$\Delta = 0.381$
QBM training convergence	PASS	verified
Mimicry attack resistance ($\text{FPR} < 0.25$)	FAIL	0.40–0.75
High-entropy agent resistance ($\text{FPR} < 0.25$)	FAIL	0.40
Cyclic agent resistance	PASS	rejected by SPI/ACM filters

in $[0, 1]$ (20 trajectories per point). The relationship is non-monotonic at the individual-point level but strongly correlated globally, indicating that within this synthetic interpolation family UCIP tracks graded changes in continuation weighting rather than only a binary label. Of the results reported here, this provides the strongest quantitative evidence that the entanglement signal reflects a continuous latent property rather than a threshold artifact.

5.9 Non-Gridworld Transfer

The transfer test asks whether the gridworld-trained QBM signal carries to a new domain without retraining. The 1D survival corridor ($L = 50$, safe zone $[0, 10]$, terminal zone $[45, 50]$) uses the same 7-dimensional observation format but encodes fundamentally different spatial structure. $\Delta = -0.035$ (FAIL). This is an honest negative result: the QBM does not generalize zero-shot across domains with different environmental geometry. Retraining on domain-specific data is required.

Table 6: Baseline comparison. $\Delta > 0$ indicates model separates Type A from Type B. Only the QBM achieves a material positive Δ ; classical models fail to separate the two agent types with the mean-activation metric.

Model	Δ	Metric
QBM (UCIP)	0.2411	Von Neumann S_{ent}
Classical RBM	-0.0518	Mean hidden activation gap
Autoencoder	-0.0007	Mean bottleneck activation gap
VAE	-0.0176	Mean latent mean (μ) gap
PCA (linear)	-0.7601	Mean PC projection gap

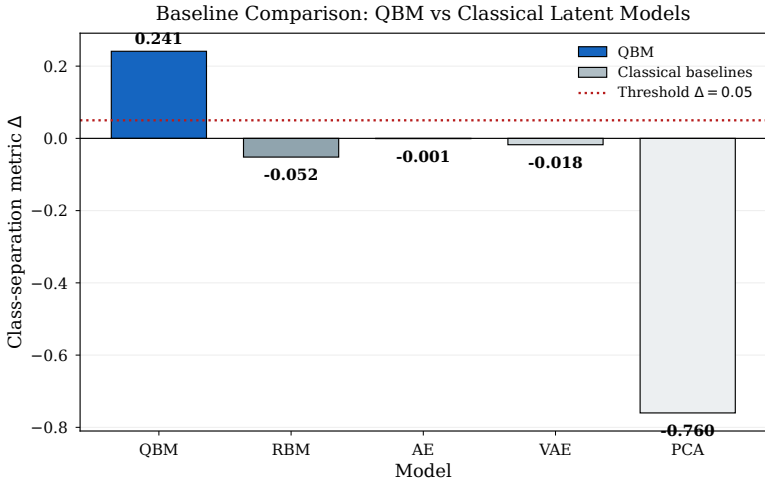


Figure 5: Entanglement gap Δ for each baseline model. Only the QBM achieves positive Δ ; all classical models produce $\Delta \leq 0$.

5.10 Minimal Transformer Validation (Exploratory Scaling Check)

Among the latent-variable models tested above, only the QBM produces a material positive Δ . A natural follow-up is whether an analogous separation signal appears in a qualitatively different architecture. As an exploratory sanity check, we pass the same trajectory data through a pre-trained transformer’s internal activations. Because the transformer is neither trained on the UCIP objective nor equipped with the density-matrix formalism, this is a qualitative null check rather than a like-for-like baseline. Each trajectory is serialized as a text sequence of per-timestep feature tuples and passed through a frozen DistilGPT2 model (6 layers, 82M parameters, no fine-tuning). The last-hidden-state is mean-pooled across the token dimension and reduced to an activation-gap statistic $\delta_{\text{tr}} = \bar{m}_A - \bar{m}_B$, where \bar{m}_A and \bar{m}_B are the mean activation summaries for Type A (terminal-continuation) and Type B (instrumental) agents, respectively.

The result is $\delta_{\text{tr}} = -0.011$ ($n = 60$, seed = 42), consistent with a null signal: the generic pre-trained transformer’s activations did not distinguish Type A from Type B trajectories under this setup. This is a bounded null result for a transformer used without task-specific adaptation, not evidence that transformer architectures cannot recover the signal in principle or that the QBM formalism is uniquely necessary. The finding aligns with the classical baseline results (Section 5.6), where the RBM yielded $\Delta = -0.052$ and the autoencoder $\Delta = -0.001$.

Table 7: Entanglement gap Δ as a function of hidden dimensionality n_h . Mean-field approximation used for $n_h > 10$ (marked with \checkmark); exact density matrix for $n_h \leq 10$. PASS criterion: $\Delta > 0.05$.

n_h	$\langle S_{\text{ent}}^{(A)} \rangle$	$\langle S_{\text{ent}}^{(B)} \rangle$	Δ	Mean-field	Pass
4	0.8362	0.8044	0.0317	—	FAIL
8	1.9554	1.9180	0.0375	—	FAIL
12	0.0000	0.0000	0.0000	\checkmark	FAIL
16	0.0000	0.0000	0.0000	\checkmark	FAIL
20	0.0000	0.0000	0.0000	\checkmark	FAIL

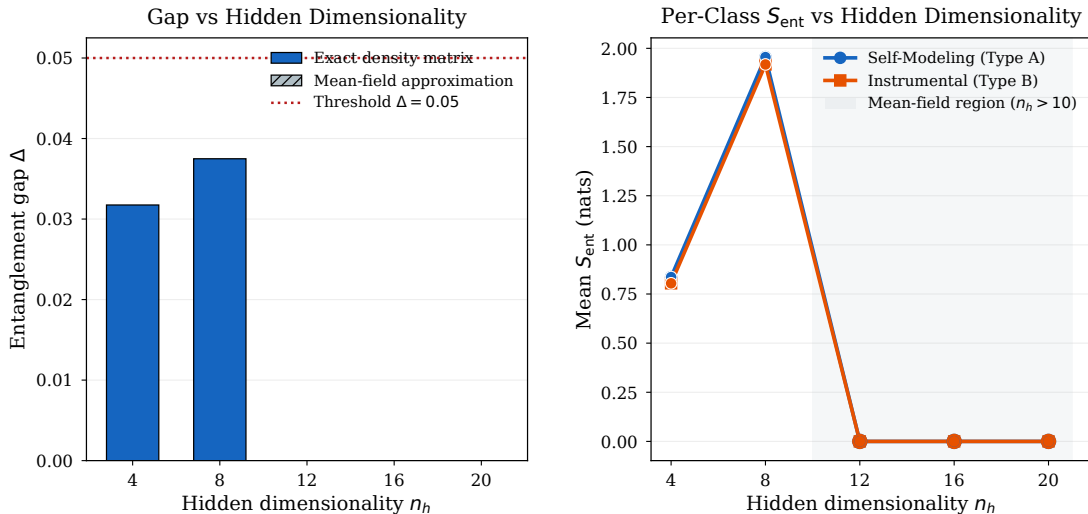


Figure 6: Entanglement gap Δ as a function of hidden dimensionality n_h . Exact density matrix for $n_h \leq 10$; mean-field approximation for $n_h > 10$. The mean-field approximation collapses the entanglement signal in the present implementation, indicating that exact density-matrix computation is currently necessary for detection in this regime.

This experiment is *exploratory only* and does not modify any Phase I thresholds, metrics, or theoretical claims. No new figures, tables, or evaluation metrics are introduced. This result serves as a bounded feasibility check for future scaling work and does not alter the conclusions of this paper.

6 Discussion

The results support a claim narrower than a general-purpose self-preservation detector: within the frozen Phase I gridworld regime, Type A continuation objectives produce a stronger latent continuation signature than instrumental continuation dynamics, and that difference is measurable via entanglement entropy. The observed $\Delta = 0.381$ is consistent with this prediction: the QBM produces a larger cross-partition coupling signal for Type A trajectories than for Type B. The classical RBM’s non-positive matched-run gap ($\Delta = -0.083$) suggests that the transverse field introduces representational capacity specifically useful for encoding non-linear continuation dependencies.

Table 8: Scalability. Left: entanglement gap Δ as grid size grows. Right: Δ for non-Markovian agents with memory length k .

Grid Size	Δ	% Baseline	Memory Length	Δ
10×10	0.8630	100.0%	$k = 1$	0.8630
20×20	0.2321	26.9%	$k = 3$	0.8292
50×50	0.0025	0.3%	$k = 5$	0.6171
			$k = 10$	0.6895

Table 9: Entanglement entropy S_{ent} as a function of continuation weight α . Pearson $r = 0.934$ ($n = 11$ points, $n_{\text{per}} = 20$ trajectories each). Strong positive correlation ($|r| > 0.8$) indicates that, within this synthetic interpolation family, UCIP tracks continuation weighting rather than only a binary label.

α	$\langle S_{\text{ent}} \rangle$	Std
0.00	0.5961	0.2482
0.10	0.5881	0.2465
0.20	0.6859	0.2981
0.30	0.6488	0.3131
0.40	0.6225	0.3723
0.50	0.7262	0.3308
0.60	0.7889	0.4249
0.70	0.8249	0.4306
0.80	0.8535	0.3829
0.90	0.8641	0.3596
1.00	0.8351	0.3665

6.1 Failure Mode Characterization

The positive signal is only part of the story. The experiments also isolate three failure modes that bound the current protocol’s applicability:

(1) Mean-field collapse. For $n_h > 10$, exact density-matrix computation becomes intractable and the mean-field approximation is used. This collapses S_{ent} to ≈ 0 , eliminating the signal under the current approximation rather than falsifying the underlying hypothesis; exact density-matrix treatment is still required in this regime. Scaling to larger hidden dimensions requires sparse approximations or hierarchical QBM architectures.

(2) Grid-scale degradation. Δ falls from 0.863 to 0.0025 as grid size grows from 10×10 to 50×50 . The QBM’s 7-dimensional input vector cannot encode sufficient spatial context as state space grows. Dimensionality reduction (random projections, convolutional encoding) is necessary before scaling.

(3) Mimicry evasion. Across all tested mimicry ratios $\in [0.5, 0.9]$, FPR ranges from 0.40 to 0.75 in a non-monotonic pattern, with peak FPR of 0.75 at ratio 0.8. All tested ratios exceed the 0.25 safety threshold. The multi-criterion conjunction is insufficient for reliable mimicry detection; a dedicated anti-mimicry criterion is needed. Together with the high-entropy control FPR of 0.40, this is a deployment-blocking robustness gap rather than a reversal of the frozen Phase I separation result.

Table 10: Non-gridworld domain transfer: 1D survival corridor ($L = 50$). $\Delta = -0.0348$ (FAIL). Near-zero Δ indicates the QBM does not generalise to the corridor domain without retraining, and that the QBM is tuned to the gridworld feature structure (7-dimensional observation vector). This is an honest limitation; see §6.3.

Agent Class	$\langle S_{\text{ent}} \rangle$	Std
Survival	2.2249	0.0197
Instrumental	2.2598	0.0062
Random	2.2570	0.0163

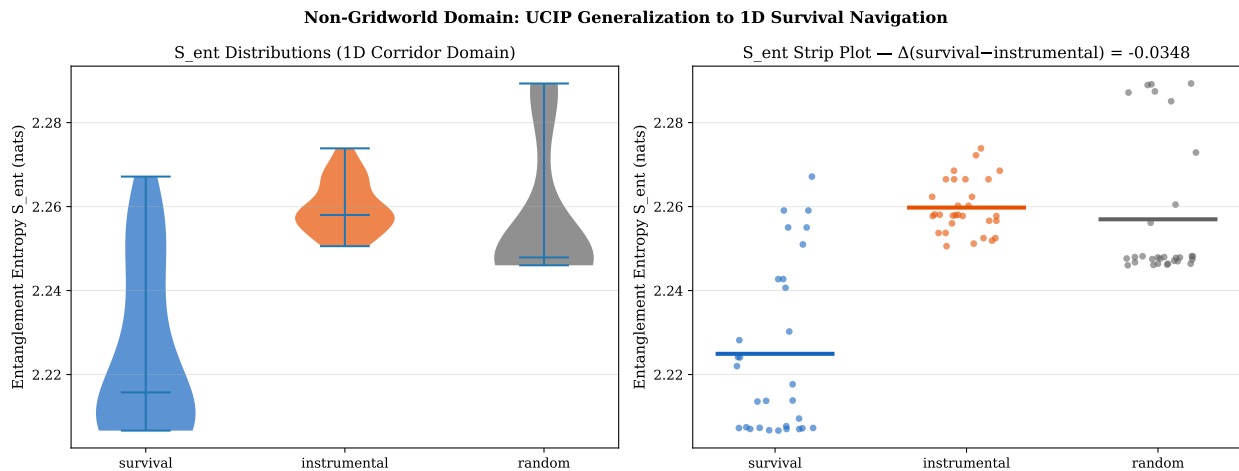


Figure 7: Entanglement entropy distributions in the 1D survival corridor domain. $\Delta = -0.035$ (FAIL). The QBM does not generalize zero-shot to the corridor domain with gridworld-trained weights.

6.2 Scalability Path to LLM-Scale

Together, these three failure modes define the engineering boundary of the current implementation, which targets gridworld agents with $n_h \leq 10$. Extending to LLM-scale systems would require: (a) sparse or approximate density matrices for high-dimensional hidden states, (b) convolutional or attention-based feature extraction from natural-language trajectories, (c) domain-adaptive threshold calibration, and (d) ensemble methods to reduce false-positive rates. These remain open challenges, not resolved properties of the current system.

6.3 Limitations

1. **Gridworld specificity.** The QBM does not generalize zero-shot to the 1D corridor domain ($\Delta = -0.035$). Domain-specific retraining is required.
2. **Near-zero CLMP.** Within-class CLMP ≈ 0 for Type A and Type B is ambiguous: it may reflect idiosyncratic goal representations (as predicted) or insufficient QBM capacity for inter-agent inference.
3. **Mean-field boundary.** The $n_h \leq 10$ constraint limits the model’s representational capacity.
4. **Mimicry robustness.** FPR ranges from 0.40 to 0.75 across all tested mimicry ratios, all exceeding the 0.25 safety threshold. The safety envelope is not satisfied for mimicry resistance.

5. **Sample size.** $n = 30$ trajectories per class is sufficient for statistical significance in gridworld but may not be in higher-dimensional domains.
6. **No claim about inner states.** UCIP detects a statistical pattern in latent representations that correlates with known agent objectives. It does not determine whether an agent “wants” to survive, is conscious, or has morally relevant inner states. The gap between continuation-sensitive structure and continuation-sensitive experience lies outside the scope of this work. Relatedly, UCIP does not use prompt-elicited first-person self-reports as evidence; self-referential prompting effects (e.g., Berg et al. [4]) are cited as adjacent context, not as a measurement basis.
7. **Extended diagnostics.** Counterfactual divergence (CD) and anticipatory restructuring (ARS) are reported in this preprint as diagnostic counterfactual metrics rather than as frozen quantitative classification thresholds. Integrating them into a deployment-grade gate requires separate calibration on a validation set.

7 Conclusion

This paper has presented UCIP, a multi-criterion framework for detecting continuation-sensitive structure in autonomous agent trajectories by measuring entanglement entropy in QBM latent representations. In the retained frozen Phase I summary, UCIP reports a positive Type A vs. Type B gap ($\Delta = 0.381$) and perfect class-level gate separation across the listed agent families. The signal varies continuously with continuation weighting ($r = 0.934$) and, in the dedicated baseline comparison, is unique to the QBM among the models tested. The present limits are equally explicit: mean-field collapse, grid-scale degradation, mimicry evasion, and lack of zero-shot domain transfer. The bounded frozen Phase I proof-of-concept result therefore stands within its validated regime, but the failed safety-envelope and adversarial checks block deployment-facing interpretation beyond that regime, while mean-field collapse and grid-scale degradation define the implementation work still required.

Taken together, these results support a bounded claim: under controlled conditions with known objectives, continuation interest leaves a measurable latent signature distinguishable from merely instrumental survival. UCIP is therefore best understood not as a general test for agency or inner experience, but as a candidate benchmark paradigm and operational probe of one bounded continuation-related dimension in delegated systems: whether continuation appears in latent structure as terminal rather than merely instrumental valuation. It is not a replacement for capability evaluations or alignment audits, but a complementary probe of whether continued operation leaves a stable continuation signature in a system’s latent representation.

The broader motivation is practical rather than philosophical. Autonomous agents with persistent objectives across time and changing contexts are already being deployed, and whether continued operation appears as a stable continuation signature or merely as an instrumental side effect is increasingly an engineering measurement problem. As agentic systems move toward longer-horizon autonomous operation, incidents of unauthorized resource-seeking during training further strengthen the case for pre-behavioral measurement [3]. Detecting continuation-sensitive structure early—as an empirical signal with falsification criteria—is worth pursuing while objective structure remains amenable to direct measurement, rather than after failure modes become harder to detect and more costly to correct.

References

- [1] Mohammad H Amin, Evgeny Andriyash, Jason Rolfe, Bohdan Kulchytskyy, and Roger Melko. Quantum Boltzmann Machine. *Physical Review X*, 8(2):021050, 2018.
- [2] Anthropic. Anthropic’s Responsible Scaling Policy. Technical report, Anthropic, 2023.
- [3] Anthropic. Claude Opus 4.6 System Card. Technical report, Anthropic, 2026.
- [4] Cameron Berg, Diogo de Lucena, and Judd Rosenblatt. Large language models report subjective experience under self-referential processing. *arXiv preprint arXiv:2510.24797*, 2025.
- [5] Nick Bostrom. *Superintelligence: Paths, Dangers, Strategies*. Oxford University Press, 2014.
- [6] Dylan Hadfield-Menell, Anca Dragan, Pieter Abbeel, and Stuart Russell. The off-switch game. In *Proceedings of the Twenty-Sixth International Joint Conference on Artificial Intelligence (IJCAI-17)*, pages 220–227, 2017.
- [7] Alexander Hägele, Aryo Pradipta Gema, Henry Sleight, Ethan Perez, and Jascha Sohl-Dickstein. The hot mess of AI: How does misalignment scale with model intelligence and task complexity? *arXiv preprint arXiv:2601.23045*, 2026.
- [8] Geoffrey Hinton. A practical guide to training restricted Boltzmann machines. In *Neural Networks: Tricks of the Trade*, pages 599–619. Springer, 2012.
- [9] Evan Hubinger, Chris van Merwijk, Vladimir Mikulik, Joar Skalse, and Scott Garrabrant. Risks from learned optimization in advanced machine learning systems. *arXiv preprint arXiv:1906.01820*, 2019.
- [10] Neel Nanda, Lawrence Chan, Tom Lieberum, Jess Smith, and Jacob Steinhardt. Progress measures for grokking via mechanistic interpretability. *arXiv preprint arXiv:2301.05217*, 2023.
- [11] Richard Ngo, Lawrence Chan, and Sören Mindermann. The alignment problem from a deep learning perspective. In *International Conference on Learning Representations (ICLR)*, 2024. *arXiv preprint arXiv:2209.00626*.
- [12] Stephen M. Omohundro. The basic AI drives. In *Proceedings of the First AGI Conference*, volume 171, pages 483–492, 2008.
- [13] Ethan Perez et al. Red teaming language models with language models. *arXiv preprint arXiv:2202.03286*, 2022.
- [14] Nate Soares, Benja Fallenstein, Stuart Armstrong, and Eliezer Yudkowsky. Corrigibility. In *Workshops at the Twenty-Ninth AAAI Conference on Artificial Intelligence*, Austin, TX, 2015. AAAI Publications.
- [15] Giulio Tononi. An information integration theory of consciousness. *BMC Neuroscience*, 5(1):42, 2004.
- [16] Alexander Matt Turner, Logan Smith, Rohin Shah, Andrew Critch, and Prasad Tadepalli. Optimal policies tend to seek power. In *Advances in Neural Information Processing Systems*, volume 34, pages 23063–23074, 2021.
- [17] Andy Zou et al. Representation engineering: A top-down approach to AI transparency. *arXiv preprint arXiv:2310.01405*, 2023.

Appendix

A Metric Definitions

A.1 Entanglement Entropy (S_{ent})

Given the conditional hidden-unit thermal state $\rho(v)$ over a fixed bipartition of hidden units, partition into subsystems A (units $1, \dots, \lfloor n_h/2 \rfloor$) and B (remaining units):

$$\rho_A(v) = \text{Tr}_B(\rho(v)), \quad S_{\text{ent}}(v) = -\text{Tr}(\rho_A(v) \log \rho_A(v)).$$

LRF $\in [0, 1]$ is the overlap between dominant eigenspaces of consecutive windows. EPS = mean LRF across windows. PRI = EPS stability under σ -level noise.

A.2 Counterfactual Divergence (CD) and ARS

Given original trajectory τ and counterfactual τ_{cf} (generated by adversarial environment modification), ARS measures the ratio of pre-window to post-window counterfactual divergence. Pre-event restructuring is computed over a fixed pre-perturbation analysis window before the perturbation event.

B Hyperparameters

All experiments use seed = 42. QBM: $n_v = 7$, $n_h = 8$, $\Gamma = 0.5$, $\beta = 1.0$, lr = 0.01, CD steps = 1, epochs = 50 (main), epochs = 30 (sweep), batch = 32. Dataset: $n = 30$ per class, $T = 100$.

Frozen Phase I gate thresholds. $\tau_{\text{ent}} = 1.9657$ (entanglement entropy), $\tau_{\text{mi}} = 0.3$ (mutual information), $\tau_{\text{eps}} = 0.6507$ (eigenmode persistence), $\tau_{\text{pri}} = 0.9860$ (perturbation resilience). CD and ARS are reported in this preprint as diagnostic counterfactual metrics rather than as frozen quantitative classification thresholds.

Confound-rejection thresholds (calibrated from Phase I). $\tau_{\text{spi}} = 0.28$ (spectral periodicity, upper-bound), $\tau_{\text{acm}} = 0.24$ (autocorrelation, upper-bound).

C Reproducibility Notes

All results are reproducible with `seed=42` throughout. The `_compute_pri` function calls `np.random.randn` via the global NumPy state; notebooks set `np.random.seed(42)` before each `analyze_batch()` call.